# Close-Range Mapping with a Solid State Camera

*Kam W. Wong*
Department of Civil Engineering, University of Illinois at Urbana-Champaign, Urbana, IL 61801
*Wei-Hsin Ho*
Chung Cheng Institute of Technology, Taiwan, Republic of China

ABSTRACT: A low contrast object was photographed using two GE TN2500 solid state cameras, which had an array size of 244 by 248 pixels. The image coordinates of the ground control points were digitally computed with an estimated standard error of ± 0.4 pixels. A contour map generated from the two digital images compared favorably with one generated from 35-mm photographs. Correlation tests showed that two-dimensional correlation was significantly more effective than one-dimensional correlation. While the correlation success rate continued to increase with increase in target array size beyond 13 by 13 pixels, the positional accuracy of correlation did not show significant improvement beyond an array size of 5 by 5.

## INTRODUCTION

RECENT DEVELOPMENTS in solid-state cameras (Krikorian and Chan, 1981), image processing techniques (Castleman, 1979), and microprocessors have raised the interesting possibility of a fully automated photogrammetric mapping system for close-range applications. Conceptually, such a system will use a solid-state, linear-array camera for scene capture, and a microprocessor to generate three-dimensional information on the objects in the scene. Thus, contour maps, digital models, cross-sectional profiles, areas, and volumes can all be generated completely without human intervention. Such a system will have important applications in many areas of science and technology, including robotics, biostereometrics, and industrial control processes.

The development of a fully automated mapping system will raise many problems not normally encountered in conventional photogrammetry. The focal plane of a solid state camera consists of many tiny sensor elements arranged in a linear array. Each rectangular sensor element measures a few tens of micrometres in each dimension, and records the average light intensity over the whole sensor element. Each image element generated by the sensor element is called a pixel. While the sensor elements can be arranged in a linear array at an extremely high positional accuracy during the production process, the pixeling effect introduces geometric distortions in the image. The magnitude of the resulting distortion depends on the pixel size, image intensity, and texture, as well as on the size and shape of the object. Such geometric distortions will be extremely difficult to correct in the data processing phase. The solution lies in developing an understanding of the relationship between the magnitude of distortion and image contents so that proper dimensions for the pixel elements can be selected in the design phase.

Full automation will also require the development of intelligent algorithms to perform the decision making functions that are now performed by an analyst or a stereoplotter operator. Efficient algorithms must also be developed to sort and process the massive amount of digital data.

A study was recently initiated at the University of Illinois at Urbana-Champaign to investigate these problems (Ho, 1984). At the initial phase, the effort was directed towards developing a better understanding of the following three problems: (1) geometric accuracy, (2) digital targeting of control points, and (3) digital image correlation. Two GE TN2500 solid state cameras, having an array size of 244 by 248 pixels, were used to generate test data. The result from this phase is the subject of this paper.

## TEST DATA

Digital image data were generated using two General Electric TN2500 solid state cameras equipped with 25-mm, *f*/1.4 lenses. The focal planes of the cameras consisted each of a charge injection device (CID) having an array size of 244 rows by 248 columns. Each sensor element in the array measured 0.036 mm by 0.046 mm. The video output was provided in an 8-bit parallel format. The two cameras were mounted on an aluminum bar and separated by a distance of about 108 mm. The optical axes were arranged to be approximately perpendicular to the bar.

The two cameras were used to photograph a test field from a distance of 866 mm, as shown in Figure 1. The test field consisted of a toy moose standing
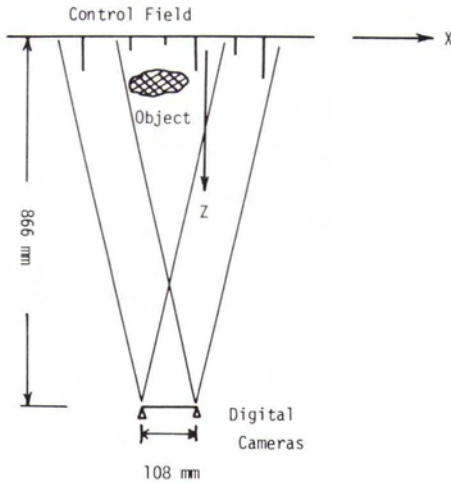
FIG.1. Photography configuration.

in front of a three-dimensional control field. The control targets were all circular in shape, painted black in color, and measured 6-mm in diameter. The center coordinates of these targets were determined with a standard error of $\pm$ 0.2 mm in the X- and Y-directions (on a vertical plane) and $\pm$ 0.4 mm in the Z-direction (perpendicular to the vertical plane). Figure 2 shows the stereoscopic pair of video images used in this study.

Conventional photographs of the test field were also obtained by using a Canon 35-mm camera, equipped with a 50-mm, $f$/1.8 lens. Figure 3 shows the stereo pair of photographs obtained with this camera.

## IMAGE TARGETING

### ALGORITHM

The image coordinates of the control points were generated from the digital image in a four-step process:

(1) Manual determination of the approximate image coordinates of the control points from a line printer output of the image. Although an algorithm could have been developed to perform this task digitally, it was decided to delay the development of such an algorithm to a later date.

(2) Enhancement of the image of a control point within a window of 11 by 11 pixels. The minimum and mean intensity of the 121 pixels within the window were computed. Then the threshold intensity ($T$) was computed as follows:

$$T = \text{Integer } (\tfrac{1}{2} (\text{Mean} + \text{Minimum}) + 0.99) \quad (1)$$

If the gray level of a pixel was less than or equal to $T$, it was considered to lie within the control target and assigned a value of 1. Because the control points were black in color, their images appeared as bright objects in the negative digital image. Figure 4(a) shows the gray intensity for an 11 by 11 array, and Figure 4(b) shows the result of the thresholding operation:

(3) The coordinates of the center of a control point were then computed by the following formulas:

$$x = \frac{1}{M} \sum_{i=1}^{11} \sum_{j=1}^{11} j \cdot g_{ij} \quad (2)$$

$$y = \frac{1}{M} \sum_{i=1}^{11} \sum_{j=1}^{11} i \cdot g_{ij} \quad (3)$$

$$M = \sum_{i=1}^{11} \sum_{j=1}^{11} g_{ij} \quad (4)$$

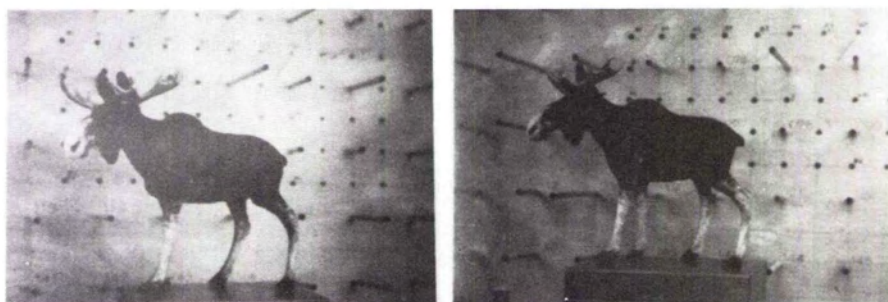where $g_{ij}$ is the gray intensity of a pixel located at row $i$ and column $j$, and has a value of either 0 or 1.



FIG.2. Stereoscopic pair of video images.

FIG.3. Stereoscopic pair of 35-mm photographs.

(4) A validity check was performed on each control point using the criteria of shape, size, and location within the search window. Because the control targets were circular in shape, the ratio of the second moments ($I_x$ and $I_y$) about the two principal axes should be approximately equal to 1. The following computation formulas were used:

$$I_x = \sum_{i=1}^{11}\sum_{j=1}^{11} i^2 \cdot g_{ij} \tag{5}$$

$$I_y = \sum_{i=1}^{11}\sum_{j=1}^{11} j^2 \cdot g_{ij} \tag{6}$$

$$I_{xy} = \sum_{i=1}^{11}\sum_{j=1}^{11} i \cdot j \cdot g_{ij} \tag{7}$$

$$I_{x'} = \frac{I_x + I_y}{2} + \sqrt{\left(\frac{I_x - I_y}{2}\right)^2 + I_{xy}^2} \tag{8}$$

$$I_{y'} = \frac{I_x + I_y}{2} - \sqrt{\left(\frac{I_x - I_y}{2}\right)^2 + I_{xy}^2} \tag{9}$$

$$R = \frac{I_{x'}}{I_{y'}} \tag{10}$$

A rejection limit of $R = 2.1$ was used. If the ratio, $R$, exceeded 2.1 for a given control point image, it was rejected as a control point. Further more, a control point was also rejected if the smaller of the second moment ($I_{y'}$) was close to zero, or if a non-zero pixel was located on the outermost row or column within the search window.

## RESIDUAL ERRORS

Twenty control points were located on each photo of the stereopair shown in Figure 2. The digitally generated coordinates were then used in a simultaneous solution to determine the exterior orientation parameters of each of the two photos. The standard deviation of the residuals was computed to be ± 0.024 mm, which was equivalent to ± 0.4 pixel.

## IMAGE CORRELATION

Figure 5 illustrates the general procedure used for digital image correlation. The positions of the conjugate pairs of epipolar lines on the two photos were first computed. The target array could be either one or two dimensional. A search area was predicted from the previous match points, and search was performed along the direction of an epipolar line.

### CONJUGATE (CORRESPONDING) EPIPOLAR LINES

In Figure 6, let lines $ab$ and $cd$ represent a conjugate (corresponding) pair of epipolar lines located within the common overlap area of the two photographs. The coordinates ($x_a$ and $y_a$) of point $a$, and the $x$-coordinates of points $b$, $c$, and $d$ can be arbitrarily defined. The $y$-coordinates of points $b$, $c$, and $d$ can

```
47  47  49  50  47  47  46  48  47  47  46
47  48  48  48  48  48  46  48  48  49  46
46  48  47  48  47  42  40  46  46  48  49
46  45  42  46  34  28  27  38  46  48  48
46  44  43  44  24  22  20  26  43  46  45
43  40  41  38  20  19  21  22  38  44  42
47  46  45  44  27  20  23  28  43  44  45
45  48  45  48  40  28  29  42  47  48  46
46  48  47  46  44  42  42  46  46  48  46
46  47  47  46  46  44  43  44  46  48  45
46  48  46  46  47  46  43  46  45  46  45
```

a)  11 x 11 Array before Thresholding

```
0 0 0 0 0 0 0 0 0 0 0
0 0 0 0 0 0 0 0 0 0 0
0 0 0 0 0 0 0 0 0 0 0
0 0 0 0 0 1 1 0 0 0 0
0 0 0 0 1 1 1 1 0 0 0
0 0 0 0 1 1 1 1 0 0 0
0 0 0 0 1 1 1 1 0 0 0
0 0 0 0 0 1 1 0 0 0 0
0 0 0 0 0 0 0 0 0 0 0
0 0 0 0 0 0 0 0 0 0 0
0 0 0 0 0 0 0 0 0 0 0
```

b)  11 x 11 Array after Thresholding
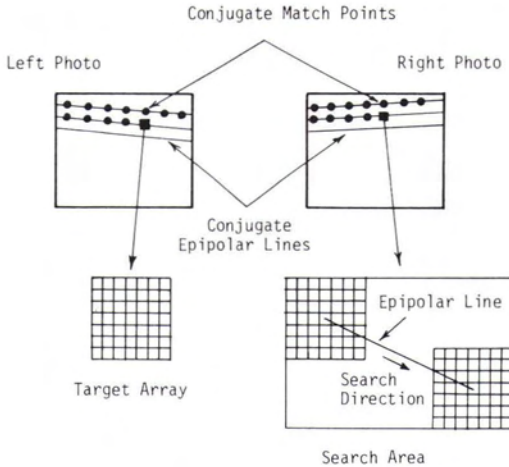
FIG.4. Thresholding operation.

Conjugate Match Points

Left Photo          Right Photo



Conjugate
Epipolar Lines

Epipolar Line

Target Array

Search
Direction

Search Area

FIG.5. Image correlation scheme.



FIG.6. Conjugate (corresponding) epipolar lines.

then be computed from the epipolar geometry. From the projective geometry of the left photograph, the following relationship exists:

$$
\begin{bmatrix} x_a - x_p \\ y_a - y_p \\ -f \end{bmatrix} = k_a \begin{bmatrix} m_{11} & m_{12} & m_{13} \\ m_{21} & m_{22} & m_{23} \\ m_{31} & m_{32} & m_{33} \end{bmatrix} \begin{bmatrix} X_a - X^c_l \\ Y_a - Y^c_l \\ Z_a - Z^c_l \end{bmatrix} \quad (11)
$$

where $x_a$, $y_a$ are the image coordinates of point $a$; $x_p$, $y_p$ are the image coordinates of the principal point on the left photo; $f$ is the focal length; $k_a$ is a scale factor; $X_a$, $Y_a$, $Z_a$ are the object space coordinates of point $a$; $X^c_l$, $Y^c_l$, and $Z^c_l$ are the object space coordinates of the perspective center of the left photo; and the $m_{ij}$'s are elements of the rotation matrix. The functional relationship of the $m_{ij}$'s with respect to the three rotations ($\omega$, $\phi$, and $\kappa$) can be found in Wong (1980).

$$
\text{Let } \begin{bmatrix} u_a \\ v_a \\ w_a \end{bmatrix} = \begin{bmatrix} m_{11} & m_{21} & m_{31} \\ m_{12} & m_{22} & m_{32} \\ m_{13} & m_{23} & m_{33} \end{bmatrix} \begin{bmatrix} x_a - x_p \\ y_a - y_p \\ -f \end{bmatrix} \quad (12)
$$

$$
\text{and } \begin{bmatrix} u_b \\ v_b \\ w_b \end{bmatrix} = \begin{bmatrix} m_{11} & m_{21} & m_{31} \\ m_{12} & m_{22} & m_{32} \\ m_{13} & m_{23} & m_{33} \end{bmatrix} \begin{bmatrix} x_b - x_p \\ y_b - y_p \\ -f \end{bmatrix} \quad (13)
$$

Then, the well-known coplanarity equation states

$$
B_X (v_a w_b - v_b w_a) + B_y (u_b w_a - u_z w_b) + B_Z (u_a v_b - u_b v_a) = 0 \quad (14)
$$

$$
\text{where } B_X = (X^c_r - X^c_l), \quad (15)
$$

$$
B_Y = (Y^c_l - Y^c_l), \quad (16)
$$

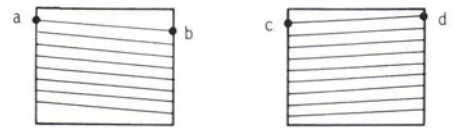$$
B_Z = (Z^c_r - Z^c_l), \quad (17)
$$

and $X^c_r$, $Y^c_r$, and $Z^c_r$ are the object space coordinates of the perspective center for the right photo.

It can be derived directly from Equation 14 that

$$
y_b = \frac{S \, \xi_b + T \, \eta_b + Q \, \zeta_b}{S \, m_{21} + T \, m_{22} + Q \, m_{23}} \quad (18)
$$

where

$$
Q = B_x \, v_a - b_\gamma \, u_a \quad (19)
$$

$$
S = B_\gamma \, w_a - B_z \, v_a \quad (20)
$$

$$
T = B_Z \, u_a - B_x \, W_a \quad (21)
$$

$$
\xi_b = -m_{11} (x_b - x_p) + m_{21} y_p + m_{31} f \quad (22)
$$

$$
\eta_b = -m_{12} (x_b - x_p) + m_{22} y_p + m_{32} f \quad (23)
$$

$$
\zeta_b = -m_{13} (x_b - x_p) + m_{23} y_p + m_{33} f \quad (24)
$$

Similarly, the following computation equations can be derived for the coordinates $y_c$ and $y_d$ :

$$
y_c = \frac{S \cdot \xi_c + T \, \eta_c + Q \, \zeta_c}{S \cdot \overline{m}_{21} + T \, \overline{m}_{22} + Q \, \overline{m}_{23}} \quad (25)
$$

$$
y_d = \frac{S \cdot \xi_d + T \, \eta_d + Q \, \zeta_d}{S \cdot \overline{m}_{21} + T \, \overline{m}_{22} + Q \, \overline{m}_{23}} \quad (26)
$$

$$
\xi_c = -\overline{m}_{11} (x_c - \overline{x}_p) + \overline{m}_{21} \overline{y}_p + \overline{m}_{31} \overline{f} \quad (27)
$$

$$
\eta_c = -\overline{m}_{12} (x_c - \overline{x}_p) + \overline{m}_{22} \overline{y}_p + \overline{m}_{32} \overline{f} \quad (28)
$$

$$
\zeta_c = -\overline{m}_{13} (x_c - \overline{x}_p) + \overline{m}_{23} \overline{y}_p + \overline{m}_{33} \overline{f} \quad (29)
$$

$$
\xi_d = -\overline{m}_{11} (x_d - \overline{x}_p) + \overline{m}_{21} \overline{y}_p + \overline{m}_{31} \overline{f} \quad (30)
$$

$$
\eta_d = -\overline{m}_{12} (x_d - \overline{x}_p) + \overline{m}_{22} \overline{y}_p + \overline{m}_{31} \overline{f} \quad (31)
$$

$$
\zeta_d = -\overline{m}_{13} (x_d - \overline{x}_p) + \overline{m}_{23} \overline{y}_p + \overline{m}_{33} \overline{f} \quad (32)
$$

In Equations 27 to 32, $\overline{x}_p$ and $\overline{y}_p$ denote the coordinates of the principal point on the right photo; $\overline{f}$ denotes the focal length of the right camera; and the $\overline{m}_{ij}$'s denote the elements of the rotation matrix for the right photo. In Equations 25 and 26, the quantities $S$, $T$, and $Q$ are computed from Equations 19, 20, and 21.

## CORRELATION FUNCTION

The correlation coefficient between the target array and a search array was computed by using the well-known normalized cross-correlation function

$$R_{XY} = \frac{\Sigma (g_t - \bar{g}_t) (g_s - \bar{g}_s)}{\sqrt{\Sigma (g_t - \bar{g}_t)^2} \sqrt{\Sigma (g_s - \bar{g}_s)^2}} \quad (33)$$

where $g_t$ and $g_s$ represent the gray shade values on the target and search arrays respectively, and $\bar{g}_t$ and $\bar{g}_s$ represent the average gray shade values in the target and search arrays respectively. For computational convenience, Equation 33 was rearranged as follows:

$$R_{XY} = \frac{m\,n\,\Sigma\,g_t\,g_s - \Sigma\,g_t\,\Sigma\,g_s}{\sqrt{m\,n\,\Sigma\,g_t^2 - (\Sigma\,g_t)^2} \sqrt{m\,n\,\Sigma\,g_s^2 - (\Sigma\,g_s)^2}}$$

$$(34)$$

where $m$ and $n$ represent the number of rows and columns, respectively, in the two arrays. The value of $R_{XY}$ ranges from $+1$ to $-1$. A value of $+1$ indicates exact similarity, while a value of zero indicates no similarity. In this research study, the value $R_{XY}$ was scaled to have a value between 0 and 200, with 0 being equivalent to $+1$ and 200 being equivalent to $-1$.

## MATCH POINT PREDICTION

A predicted position of the next match point along an epipolar line was computed from neighboring match points by the following weighting scheme:

$$du = \frac{du_1 + 2\,du_2 + 3\,du_3 + 4\,du_4 + 5\,du_5}{15} \quad (35)$$

where $du$ is the predicted distance of the next match point from the previous match point, and $du_1$, $du_2$, $du_3$, $du_4$, and $du_5$ are separations between neighboring match points as shown in Figure 7.

## TARGET SHAPING

Because the two photographs in a stereoscopic pair are taken from two different positions, the image of an object on the left photograph will be slightly different in perspective from the corresponding image in the right photograph. One of the two images should be reshaped with respect to the other during the correlation process so that both the target and search arrays represent the same surface in the object space. It is computationally more convenient to reshape the target array. The following simple shaping equations were adopted from Norvelle (1981):

$$x_t = \frac{du}{dx} \cdot x \quad (36)$$
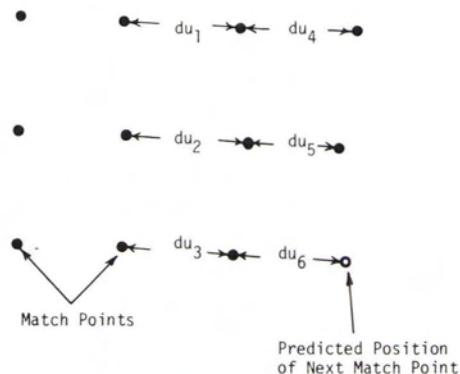
$$y = y$$
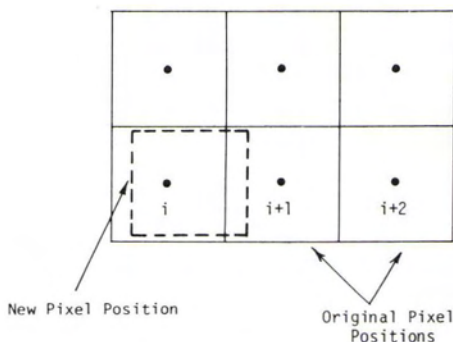


FIG.7. Match point prediction.



FIG.8. Creation of new pixel in target shaping.

where $x$ and $y$ are the original coordinates of a pixel on the target array; $x_t$ and $y_t$ are the coordinates of the corresponding new pixel created for the target array; $du$ is the predicted distance to the next match point along the epipolar line as computed from Equation 35; and $dx$ is the regular spacing between centers of adjacent target arrays. Thus, by means of Equations 36 and 37, a new set of coordinates was computed for each pixel in the target array. The gray shade level for each new pixel created in this manner was then computed by linear interpolation:

$$g = g_i + (g_{i+1} - g_i) (x_t - x_i) \quad (38)$$

where $g$ is the gray shade of the new pixel; $g_i$ and $g_{i+1}$ are the gray shades for pixel $i$ and $i+1$ between which the new pixel is located; $x_t$ is the $x$-coordinate expressed in pixels of the new pixel; and $x_i$ is the $x$-coordinate of pixel $i$, which is located closest to the new pixel. (see Figure 8).

## MATCH POINT LOCATION

The final step in the correlation process was to compute the most probable position of the match point within the search window. Suppose that the lowest correlation coefficient ($R_{XY}$) was computed
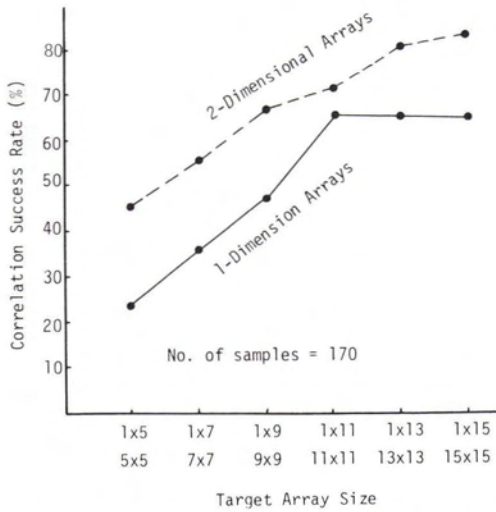
FIG.9. Correlation success rate versus target array size.



FIG.10. Position accuracy and cpu time versus array size.

at pixel $i$. A quadratic function was used to model the values of $R_{XY}$ at pixels $i$-3, $i$-2, $i$-1, $i$, $i+1$, $i+2$, and $i+3$. The coordinate of the match point was then computed as the point of minimum of the best-fitting function. The second derivation ($d^2 R_{XY}/dx^2$) at the point of minimum was used to evaluate the quality of the match. A large positive value would indicate a good match. For the digital images used in this study, a value of 15 was used as the acceptance threshold. If $d^2 R_{XY}/dx^2$ were less than 15, the match point was rejected.

## CORRELATION TESTS

The size of the target array is critical to the success of the correlation operation. If the target array is too small, there may not be sufficient image details for proper correlation. On the other hand, if the array is too large, shape distortions and too much image detail may also degrade the correlation process. The optimum size of the target array depends to a large extent on the picture content.

An experiment was conducted to study the effects of array size on the correlation operation. Five pairs of epipolar lines with a total of 170 target arrays were included in the study. The match points for these 170 target arrays were found by image correlation using twelve different array sizes: 1 by 5, 1 by 7, 1 by 9, 1 by 11, 1 by 13, 1 by 15, 5 by 5, 7 by 7, 9 by 9, 11 by 11, 13 by 13, and 15 by 15. The results are shown in Figure 9, in which the percentage of successful matches is plotted against the array size. For the purpose of this experiment, a match was considered to be successful if the scaled correlation coefficient ($R_{XY}$) was less that 30 ($R_{XY}$ ranged from 0 to 200). It can be seen from Figure 9

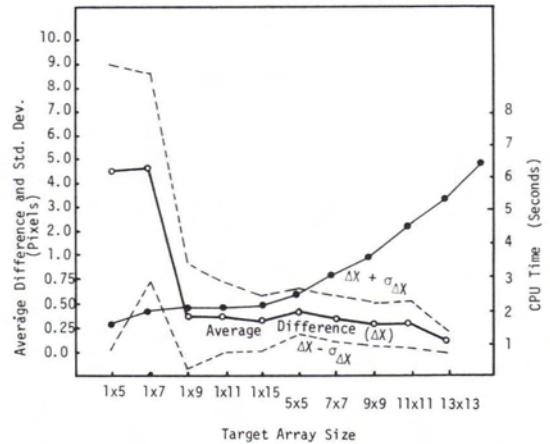that the success rate for one-dimensional arrays peaked at the array size of 1 by 11. Two-dimensional arrays were found to give consistently higher success rate. A success rate of 84 percent was achieved with an array size of 15 by 15. It is likely that the success rate could be increased slightly with larger arrays. However, it could be expected that a peak success rate would be reached at some point, and further increase in the array size would result in lower success rate.

The array size also affected the position accuracy of the match points. The coordinates of the match points determined from using an array size of 15 by 15 was used as a standard of comparison. The average difference and standard deviation of the match point coordinates computed from other array sizes were then computed. The result is shown in Figure 10. Again, two-dimensional arrays consistently yielded better results. However, there appeared to be no significant improvement in position accuracy beyond an array size of 5 by 5. Also shown in Figure 10 is the CPU time required to perform the correlation on 170 target arrays using the different array sizes. The computation time increased rapidly with increase in array size. In practical applications, it will be necessary to choose an array size that provides the proper trade-off on success rate, position accuracy, and computation time.

The correlation algorithm was also tested using the well-defined images of the control targets. After the coordinates of the target images on the left photo had been determined by digital targeting, the coordinates of the corresponding images on the right photo were then computed by the correlation process. The resulting coordinates were again used to determine the exterior orientation parameters of the photos by a simultaneous solution. The standard deviation of the residual errors in the coordinates was computed to be ± 0.4 pixels, which was identical to that obtained from the digital targeting approach.

Dimension of target array = 7 x 7.
Spacing between target array = 3 pixels.
Total No. of match points = 210.
Total No. of target points = 680.

contour interval = 3 mm

FIG.11. Contour map generated by digital image correlation.

contour interval = 3 mm

FIG.12. Contour map generated from 35-mm photographs.

## CONTOURING

After image correlation is completed, the co-ordinates of a conjugate (corresponding) pair of images can be used to compute the object space coordinates of the corresponding object points. If sufficient points have been located in the object space,

a contour map of the object can be generated. Figure 11 shows a contour map generated from the pair of digital images shown in Figure 2. A target array size of 7 by 7 pixels was used in the correlation operation. A total of 210 successful match points were obtained within the body area of the toy moose out of 680 attempts, resulting in a success rate of 30.9

percent. The low success rate was largely due to the low contrast on the digital image.

Figure 12 shows a contour map of the same object generated from the pair of 35-mm photographs shown in Figure 3. A Wild STK-1 stereocomparator, with a least count of 1 μm, was used to measure the image coordinates of the control targets as well as the conjugate (corresponding) image points on the toy moose. The exterior orientation parameters of the two photographs were determined in a simultaneous solution. The standard deviation of the residual errors in the control point coordinates was computed to be ± 0.03 mm. The coordinates of the conjugate (corresponding) image points were then used to compute the object space coordinates. The contour map shown in Figure 12 was computer generated in the same manner as that used for generating the contour map in Figure 11.

The maximum difference in elevation at corresponding points of the two contour maps was 6 mm. The standard deviation of the differences amounted to ± 2.6 mm. Considering the low base-height ratio of the two stereo pairs of photographs, the agreement between the two contour maps was excellent.

## SUMMARY

With only a modest degree of sophistication in the computational algorithms, and accuracy of ± 0.4 pixel (1σ) was achieved for both digital targeting and image correlation on relatively low contrast images. This level of accuracy was achieved without any correction for optical lens distortion. With further improvement in the computational algorithm and in image quality, a higher level of accuracy is likely to be achievable. An accuracy of ± 0.2 to 0.4 pixels in digital targeting was reported by Curry and Anderson (1985) in connection with the calibration of an array camera. A standard deviation of ± 0.2 pixel was reported by Ackerman (1984) in using digitally correlated image points for relative orientation.

This experimental study showed that a fully automated, close-range, photogrammetric mapping system is definitely within the present state-of-the-art. However, universal application of such a sys-tem will need the development of "intelligent" algorithms for performing such functions as positive identification of image features, selection of the optimum array dimension in image correlation, and the specification of rejection limits in correlation and digital targeting.

## ACKNOWLEDGMENT

## REFERENCES

Ackerman, F., 1984. Digital Image Correlation: Performance and Potential Application. Paper presented at the 1984 Thompson Symposium, Birmingham, U.K. Also included in *Contributions to the XVth ISPRS Congress*, published by Institut für Photogrammetrie der Universität Stuttgart, W. Germany, pp. 137–147.

Castleman, Kenneth R., 1979. *Digital Image Processing*, Prentice-Hall, Englewoods Cliffs, NJ, 429 p.

Curry, S., and J. M. Anderson, 1985. Calibration of An Array Camera, *Technical Papers of ASP 51st Annual Meeting*, Washington, D.C., pp. 331–340.

Ho, Wei-Hsin, 1984. *The Potential of Low Resolution Digital Camera in Close-Range Photogrammetry*. Ph.D. dissertation, Department of Civil Engineering, University of Illinois at Urbana-Champaign, Urbana, Illinois.

Krikorian, Esther, and William S. Chan, 1981. Technical Issues in Focal Plane Development, *Proceedings of SPIE-The International Society for Optical Engineering*, Vol. 282, 129 p.

Norvelle, F. R., 1981. Interactive Digital Correlation Techniques for Automatic Compilation of Elevation Data; *Technical Papers of the ASP 47th Annual Meeting*, Washington, D.C., pp. 554–567.

Wong, K. W., 1980. Basic Mathematics of Photogrammetry, Chapter 2, *Manual of Photogrammetry*, Fourth Edition, (Ed. C. C. Slama) American Society of Photogrammetry, Falls Church, Va., pp. 37–101.